Role of the Molecular Sublayer in the Melting or Freezing of Sea Ice

MICHAEL STEELE AND GEORGE L. MELLOR

Atmospheric and Oceanic Sciences Program, Princeton University, Princeton, New Jersey

MILES G. MCPHEE

McPhee Research Co., Yakima, Washington

24 February 1988 and 25 July 1988

ABSTRACT

In an earlier paper, a second-moment turbulence closure model was applied to the problem of the dynamic and thermodynamic interaction of sea ice and the ocean surface mixed layer. An overly simplistic parameterization of the molecular sublayers of temperature and salinity within the mixed layer was used. This paper investigates the use of a more recent parameterization by Yaglom and Kader which is supported by laboratory data. A relatively low melt rate results in the case where ice overlays warm water. This agrees with some recent observations in the interior of the marginal ice zone.

A surface heat sink drives the freezing case which, due to the large difference in heat and salt molecular diffusivities, produces a strong supercooling effect. This is converted into an estimate of frazil ice production through a simple scheme. The model results provide an explanation for high frazil ice concentrations observed in the Arctic and Antarctic.

1. Introduction

Mellor et al. (1986, hereafter MMS) presented a numerical model of the ocean boundary layer under melting or freezing ice which expressed the boundary condition between the ice and the first grid point of the model in terms of a simple parameterization of the molecular boundary layer structure, following Sheppard (1958). Recent observations in the interior marginal ice zone (McPhee et al. 1987) suggest that our previous treatment significantly overestimates heat and salt fluxes at the ice–ocean interface. This note presents an updated scheme for calculating these fluxes, which draws from extensive laboratory studies of heat and mass transfer in hydraulically rough flows. We also extend the discussion of the freezing process, including effects of supercooling and frazil ice production. Relative to the results of MMS, the new scheme reduces ice–ocean fluxes, which reduces the melt rate calculated by the model for a given oceanic thermal forcing. The transient behavior of the melt rate in the present formulation also changes. In the case of freezing, the new scheme increases the tendency toward supercooling, because of the large difference between molecular heat and salt diffusivities. The latter result may be significant in explaining high frazil concentrations in sea ice, especially in the Southern Ocean, and the small but persistent supercooling observed in the Arctic (e.g., Lewis and Perkin 1983). A discussion of the new scheme is given in the next section. Section 3 presents the results for the melt case, while section 4 shows the results for the freeze case. Conclusions are discussed in section 5.

Corresponding author address: Dr. Michael Steele, Polar Science Center/APL, University of Washington, 1013 NE 40th Street, Seattle, WA 98105.

2. Parameterization of scalar surface fluxes

The equations for temperature and salinity are

$$\frac{\partial T}{\partial t} = \frac{\partial}{\partial z}\left[(K_h + \alpha_t)\frac{\partial T}{\partial z}\right] \tag{1}$$

$$\frac{\partial S}{\partial t} = \frac{\partial}{\partial z}\left[(K_h + \alpha_s)\frac{\partial S}{\partial z}\right] \tag{2}$$

where α_t and α_s are the molecular diffusivities, K_h is the turbulent diffusivity of both temperature and salinity, and $K_h \gg \alpha_t, \alpha_s$. The turbulence closure scheme of Mellor and Yamada (1982) is used to obtain K_h. The analogous momentum equations and boundary conditions may be found in MMS.

At the surface, the boundary condition for temperature is given, in part, by

$$\Phi_T \equiv \frac{T_1 - T_0}{F_T/u_\tau} = \frac{1}{\kappa}\ln\left(\frac{-z_1}{z_0}\right) + A_T \tag{3}$$

where Φ_T is nondimensional and the equation for salinity is identical, except that T is replaced by S. The surface flux is F_T, u_τ is the square root of the kinematic surface stress, and κ is the von Kármán constant, 0.4.

The temperature on the ocean side of the ice–ocean interface is T_0, (see Fig. 2 of MMS), while T_1 is the temperature at the uppermost grid point, z_1 (where the origin is at the ocean surface). The roughness length z_0 is the usual integration constant in the "constant flux" boundary layer for momentum. It is approximately $z_0 \approx h/30$, where h is the average height of "roughness elements," or in this case, ice floe draft variations; here we use the value $z_0 = 1$ cm, in keeping with MMS.

The first term on the right-hand side of Eq. (3) represents the scalar change across the portion of the boundary layer described by a constant turbulent momentum flux. However, for scalar quantities, we expect molecular effects to play a significant role close to the surface, as noted in MMS. The change across the molecular sublayer is given by the term A_T, which, following Sheppard (1958), was modeled by MMS as

$$A_T = \frac{1}{\kappa} \ln(\kappa \cdot \mathrm{Re} \cdot \mathrm{Pr}) \qquad (4)$$

where $\mathrm{Re} \equiv u_\tau z_0/\nu$, the Prandtl number $\mathrm{Pr} \equiv \nu/\alpha_t$, and ν is the molecular viscosity. [Equations (3) and (4) are equivalent to an equation where $A_T \equiv 0$ in (3) but where z_0 is replaced by $z_{0_t} \equiv \alpha_t/(ku_\tau)$.] The analogous A_S for salinity uses the Schmidt number $\mathrm{Sc} \equiv \nu/\alpha_s$ in place of Pr.

Garratt and Hicks (1973), using these formulas, found reasonable agreement with a wide variety of data for the range $5 < \mathrm{Re} < 100$. For the flows to be discussed below, $u_\tau \approx 0.01$ m s^{-1}, $z_0 = 0.01$ m, and $\nu = 1.8 \times 10^{-6}$ m^2 s^{-1}, which implies $\mathrm{Re} \approx 50$. However, Garratt and Hicks (1973) considered only atmospheric data, for which $\mathrm{Pr} \approx 1$. In the ocean, Pr = 13.8, and Sc = 2432. Thus, we expect the molecular diffusion sublayer to be more important in the ocean than in the atmosphere. These arguments and work by McPhee et al. (1987) concerning possible overestimates in the model's melt rates led to consideration of an alternate form for A_T. The formula we adopted is from Yaglom and Kader (1974) (see also Owen and Thomson 1963). For temperature, A_T is given by

$$A_T = 3.14(\mathrm{Re}^{1/2})(\mathrm{Pr}^{2/3} - 0.2) + 2.11 \qquad (5)$$

and the analogous formula for salinity uses Sc in place of Pr. Note that the above formula has a much stronger dependence on Pr (for high Pr) than the logarithmic variation in Equation (4). Hereafter, Eq. (5) shall be denoted as the YK sublayer formulation, as opposed to the Sheppard formulation of MMS. The constants were adjusted in Yaglom and Kader (1974) to a variety of data which included Pr = 13.8, but not such high values as Sc = 2432 for salt. Thus, the validity of Eq. (5) for very high Pr or Sc is still uncertain. As noted in McPhee et al. (1987), the last two constants in Eq. (5) are negligible for the Prantl numbers under consideration, so that

$$\Phi_T \approx \frac{\mathrm{Pr}_t}{\kappa} \ln\left(\frac{-z_1}{z_0}\right) + b(\mathrm{Re}^{1/2})(\mathrm{Pr}^{2/3}) \qquad (6)$$

where $b = 3.14$, and we have multiplied the logarithmic term by the turbulent Prandtl number, which is about 0.87 for both temperature and salinity. In fact, the molecular Prandtl number dependence of the second term is so strong, that the first (logarithmic) term is negligible. That is, for a given surface flux, nearly all of the temperature (or salinity) change occurs within the molecular sublayer, and very little across the log layer. Alternately, for a given temperature difference between the ice and deep water, the surface flux is much weaker when the YK sublayer is included in the boundary layer formulation. This leads to relatively low melt rates, as discussed in the next section.

3. The melting process

Melting in the MIZ is largely forced by underlying water which is above its local freezing point. In the numerical simulation now under discussion we set $T(z, t = 0) = 0$°C, which is ~2°C higher than freezing, for $S = 34$ ppt. As in MMS, a neutral Ekman layer is first spun up, with a given surface ice velocity of 20 cm s^{-1}, linearly ramped up over one inertial period to suppress inertial oscillations. At two inertial periods, melting is enabled. Figure 1 shows the response, and may be compared with Fig. 6 of MMS. Melting leads to the development of a relatively cold, fresh surface layer. However, the contrast with deeper water is much less here than in MMS. This is due to the lower melt rate, which is shown, along with the drag coefficient and veering angle, in Fig. 2. Also shown in Fig. 2 are cases in which the surface velocity is 10 and 40 cm s^{-1}. This figure may be compared with Fig. 8 of MMS. (Note that the curves were mislabeled in the caption of Fig. 8 of MMS and should conform to the labels in the caption of Fig. 2 of this paper.) As in MMS, melt water stabilizes the water column, thus inhibiting downward momentum flux and reducing the ice–ocean drag coefficient. Also, in agreement with the analytical theory of McPhee (1981), the veering angle increases. However, because the melt rate is lower, these effects are smaller than in MMS.

The main result is that the YK sublayer yields greatly reduced surface heat flux and melt rate near the leading edge of the ice (corresponding to small nondimensional time after initiation of melting). Subsequently, the melt rate returns to the MMS values. However, the mixed-layer temperature is colder here as can be seen by comparing Fig. 2 with Fig. 6 of MMS. After five inertial periods, the equilibrium melt layer temperature is about −1.0°C, while the weaker Sheppard sublayer yields melt layer temperatures near freezing. This is in accord with the marginal ice zone data of McPhee et al. (1987) who showed that bottom melting of sea ice in water with temperature several degrees above freezing was much slower than implied by the Sheppard

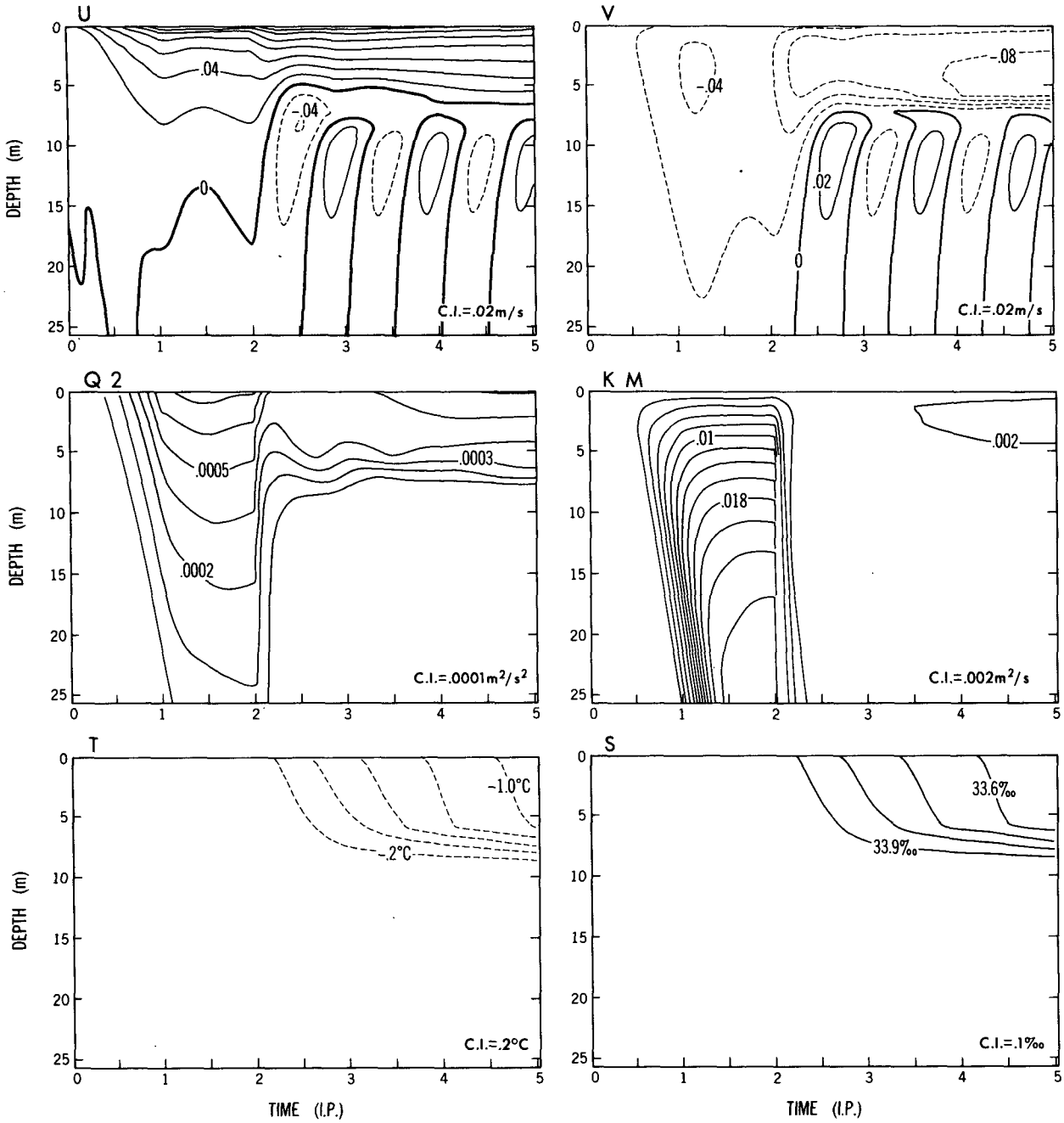

FIG. 1. Boundary layer development with melting ice where the initial temperature is 0°C, and the initial salinity is 34 ppt. The experiment is exactly the same as in MMS (see their Fig. 6), except that the YK sublayer is used. The flow is forced by an imposed surface (ice) velocity, ramped up from zero through one inertial period and then held constant at the value $(U_i, V_i) = (0.20, 0.0)$ m s^{-1}. Melting is enabled after two inertial periods. The top panels are the velocity components. The middle panels are twice the turbulence kinetic energy and the vertical eddy viscosity. The bottom panels are temperature and salinity.

sublayer; this observation prompted consideration of the new scheme. However, McPhee decided that the coefficient, $b = 1.57$, fit his data better than the value, 3.14, in (6).

We note that Josberger (1984) found very high melt rates of over 50 cm day^{-1} at the outer edge of the MIZ, in contrast to the reduced values discussed in this study. Of course, melting in this region is probably greatly affected by complications due to ocean swell and widely spaced floes.

The amount of melting is a function of the under-ice roughness, z_0. Figure 3 shows the total melted ice

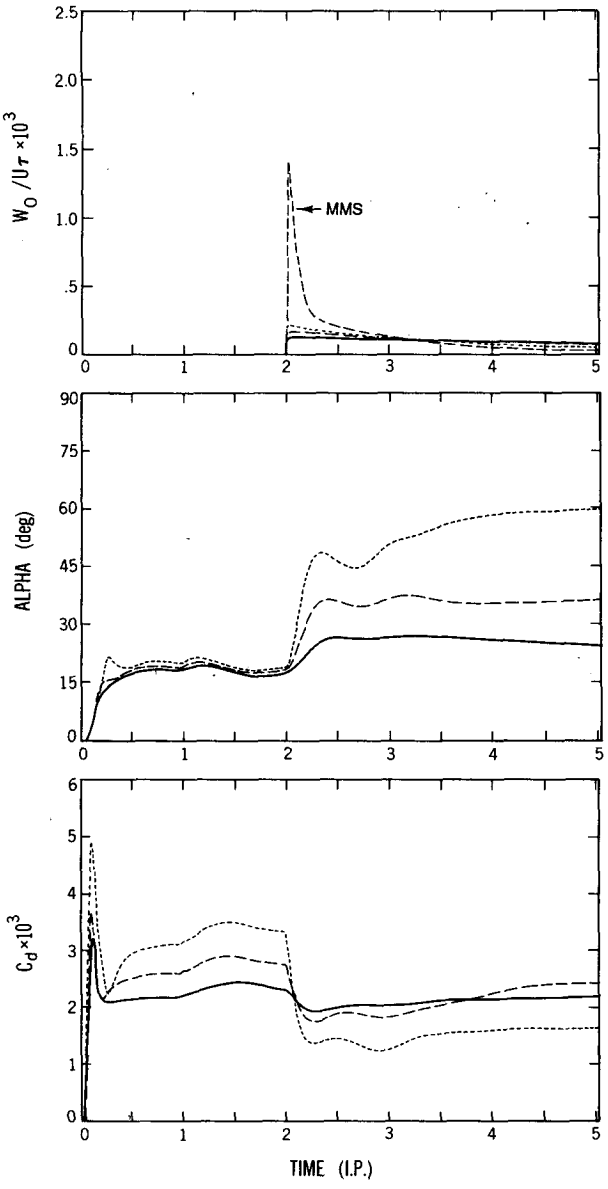

FIG. 2. The drag coefficient and angle between the surface stress and ice velocity vectors and the melt rate normalized on u_τ corresponding to Fig. 1 (long dashed lines). Also included are cases for imposed surface velocities of 0.10 (short dashed lines) and 0.40 (solid lines) m s^{-1}. Also included is a melt rate calculation from MMS for surface velocity of 0.20 m s^{-1}.

at the end of the experiment (after 1.5 days of melting) as a function of z_0 (solid line). A constant ice–ocean stress of 0.2 N m^{-2} has been imposed. Rougher ice produces less melting, because the turbulent eddies are forced to circulate farther away from the actual ice–ocean interface, where heat exchange is accomplished via molecular diffusion alone. If the molecular sublayer were ignored in this calculation, the conclusion would be exactly the opposite: increased stirring by rough ice enhances turbulent heat exchange and thus increases the melt rate. This may also be seen in Eq. (6), where the two terms on the right-hand side vary with z_0 in opposing directions. In MMS, it was mentioned that an equation analogous to their Eq. (18) could be solved for the melt rate, W_0. As in MMS, we ignore conductive heat flux through the ice; i.e., melting is forced solely by warm underlying water. Also, as mentioned previously, we may neglect the logarithmic term in Eq. (6) relative to the molecular sublayer term. The melt rate is then given by

$$W_0 \propto \frac{1}{(A_T/u_\tau)} \propto \frac{1}{(z_0/u_\tau)^{1/2}}.$$

Figure 3 shows the total melt, multiplied by $z_0^{1/2}$, for a constant ice–ocean stress of 0.2 N m^{-2} (dashed line). There is still some variation with roughness, demonstrating that W_0 is also a function of temperature and salinity in the surface layer (T_1 and S_1), which also vary with z_0.

Note that melting of initially rough ice will tend to smooth the under-surface, and so increase the melt rate. A simple parameterization of this was included in several data simulations of MMS.

4. The freezing process

As in MMS, we examine the freezing case by imposing a constant atmospheric heat sink of $\rho_0 c_{po} Q_i = 60$ W m^{-2}, which is enabled at two inertial periods. The

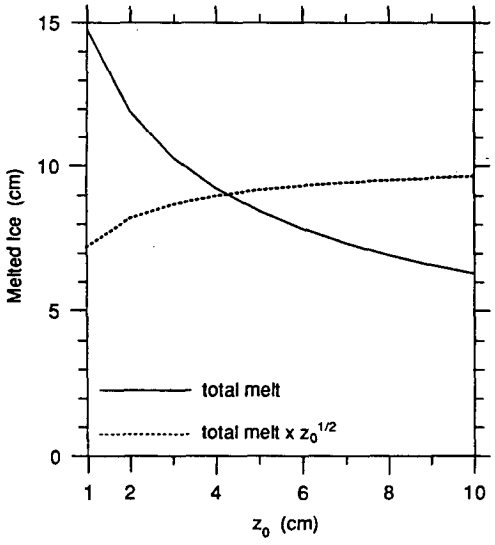

FIG. 3. The amount of melted ice at 5.0 inertial periods (after 1.5 days of melting) as a function of under-ice roughness, z_0 (solid line). The ocean is forced by a constant ice-ocean stress of 0.2 N m^{-2}. Rougher ice induces less melting, because turbulent eddies are forced to circulate farther from the ice–ocean interface, where heat exchange is accomplished via molecular diffusion alone. The melt rate is roughly proportional to $z_0^{-1/2}$ (dashed line), though the surface layer temperature and salinity also vary with z_0 and so also influence the melt rate.

flow is dynamically forced by ice velocity = (0.20, 0.0) m s^{-1}. The water salinity is initially uniform with depth, down to a halocline of 0.04 ppt (20 m)$^{-1}$ which begins at 60 m depth. The surface water in contact with the (growing) sea ice cover is located on the freezing line. At depth, however, the freezing point is depressed due to its (approximately linear) pressure dependence. The initial temperature structure is assumed constant with depth (except for the salinity dependency of the freezing point). This well-mixed condition was observed by Lewis and Lake (1971) under growing ice sheets in Antarctica. Thus, water at depth is initially slightly warmer than its local freezing point. The equation of state is

$$T_f = T_f\{S, z\} = mS + nz \qquad (7)^1$$

where $m \equiv -0.06$ ppt °C^{-1}, $n \equiv -0.000759$°C^{-1} (Fujino et al. 1974), and the vertical coordinate z is negative below the ocean surface.

The initial condition is

$$T(z) = T_f\{S(z)\}. \qquad (8)$$

The upper boundary condition T_0 is given by

$$T_0 = T_f\{S_0\}. \qquad (9)$$

Results of the calculations are shown in Fig. 4. The dynamics are only slightly affected by the freezing process. A nearly constant freeze rate of $w = 0.93$ cm day^{-1} yields 1.4 cm of ice by the end of the experiment at five inertial periods. As in the melt case, however, the surface fluxes of temperature and salinity are greatly modified by the use of Eq. (5). The YK sublayer allows the value of S_0 to build up due to salt rejection, without an appreciable flux to deeper layers. The value of T_0, which is constrained to lie on the freezing curve, thus decreases. The efficiency of the molecular diffusion of heat over salt then leads to a strong thermal flux to deeper layers, so that the water in Fig. 4 is significantly cooler than in the analogous Fig. 10 of MMS (note the contour interval for temperature).

a. *Supercooling*

As noted in section 2, the YK sublayer has a much stronger dependence on molecular Prantl (or Schmidt) number than does the Sheppard sublayer. Thus, the supercooling mechanism discussed in MMS is much more effective in the present experiment. Figure 5 shows that near the surface, water is supercooled by ~0.015°C one day after freezing begins; the analogous experiment using the Sheppard sublayer yields only ~0.0001°C supercooling. Observations of supercooling in the ocean vary over several orders of magnitude, depending on the site. Lewis and Perkin (1983) measured supercooling of ~−0.008°C in the upper 8 m of the water column north of Spitzbergen.

Note that the pressure dependence of T_f is apparent on the temperature scales we are considering. The curve is essentially linear. The freezing point is also a function of salinity, which remains nearly uniform with depth.

b. *Frazil ice*

The amount of supercooling predicted by the model is, in fact, an overestimate, due to the tendency of supercooled water to produce small in situ ice crystals, or "frazil ice," which limits the temperature drop by releasing latent heat (e.g., Omstedt and Svensson 1984). These tiny crystals of relatively fresh ice, typically several millimeters in diameter, undergo "negative sedimentation," i.e., they are buoyant with respect to their salty environment, and so rise to the surface. Eventually, the ocean surface becomes covered with a thin layer (several cm) of precipitated frazil crystals, termed "grease ice." The layer begins to decrease the ocean-to-atmosphere heat loss, as well as suppressing surface wave amplitude. This is the first stage in the formation of mature sea ice.

To properly model this phenomenon, a prognostic equation for frazil ice concentration should be included, as well as source/sink terms in the temperature and salinity equations (Omstedt and Svensson 1984). In this paper, however, the simplest scheme employed by, for example, convective cloud modelers with respect to rain water is used. That is, at each time step, the amount of supercooling at each depth implies a certain amount of frazil ice creation. In the real ocean, these crystals take some time to diffuse/convect upwards, during which they undergo accretion and contamination by sediments and biota. We calculate an upper limit on total frazil ice production by immediately precipitating out all frazil ice in the water column, at each time step. This leaves the water at the local freezing temperature, as discussed below.

The procedure is as follows. We first write mass heat and salt balances for a volume of water before and after frazil ice creation:

$$m_{w_1} = m_{w_2} + m_i \qquad (10)$$

$$m_{w_1}(c_{p_w}T_1 + L) = m_{w_2}(c_{p_w}T_2 + L) + m_i c_{p_i} T_i \qquad (11)$$

$$m_{w_1}S_1 = m_{w_2}S_2 \qquad (12)$$

where subscript 1 refers to the initial supercooled state, and subscript 2 to the final state where both water at its local freezing point and frazil ice crystals exist. The subscripts w and i refer to water and frazil ice, respectively, while m is mass and L is the latent heat of fusion. Frazil ice is created in this model by resetting $T_1 \rightarrow T_f$ at each time step. This releases a small amount of latent

[1] A more refined version is $T_f = mS + n(z - D)$, where $D = D(t)$ is the ice draft. Excluding D results in negligible change in the calculated results, since only 3 cm of (total) ice forms. The effect may be stronger when more ice is created. Also, a better value of m is −0.0543°C ppt^{-1} (McPhee et al. 1987). However, we retain the value $m = -0.06$°C ppt^{-1} for consistency with MMS.

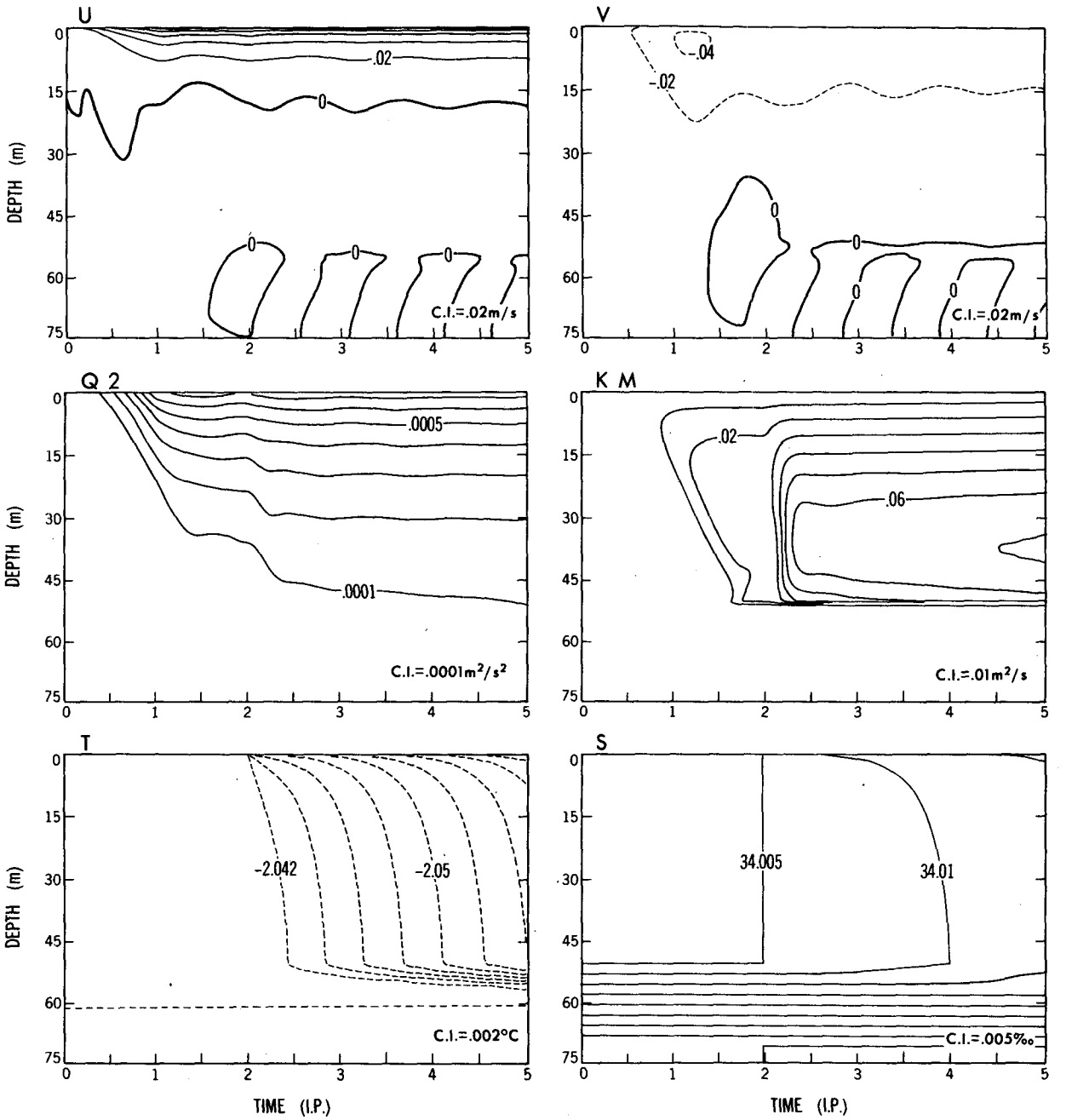

FIG. 4. Boundary layer development for freezing ice, using the YK sublayer. The initial temperature is constant at the surface freezing point of −2.041°C down to 50 m depth; below 50 m a stable pycnocline is established. The flow is forced by an imposed ice velocity, which is ramped up from zero through one inertial period and then held constant at the value $(U_i, V_i) = (0.20, 0.0)$ m s^{-1}. Heat conduction through the ice at the rate of 60 W m^{-2} is imposed after two inertial periods. The top panels are the velocity components. The middle panels are twice the turbulence kinetic energy and the vertical eddy viscosity. The bottom panels are temperature and salinity fields.

heat, as well as slightly enhancing the water's salinity. Assuming thermal equilibrium between ice and water in the final state yields $T_i = T_2$. Thus, we obtain

$$T_2 = T_1 + \gamma[\hat{L} + T_1(1 - R)] \quad (13)$$

$$S_2 = S_1(1 + \gamma) \quad (14)$$

where $\hat{L} \equiv L/c_{pw} = 79.2$°C, $R \equiv c_{pi}/c_{pw} = 0.5$, and $\gamma \equiv m_i/m_{w_1}$. In deriving Eqs. (13) and (14), terms of order γ^2 were neglected. We finally add the condition that T_2 and S_2 are on the freezing line, so that

$$T_2 = mS_2 + nz. \quad (15)$$

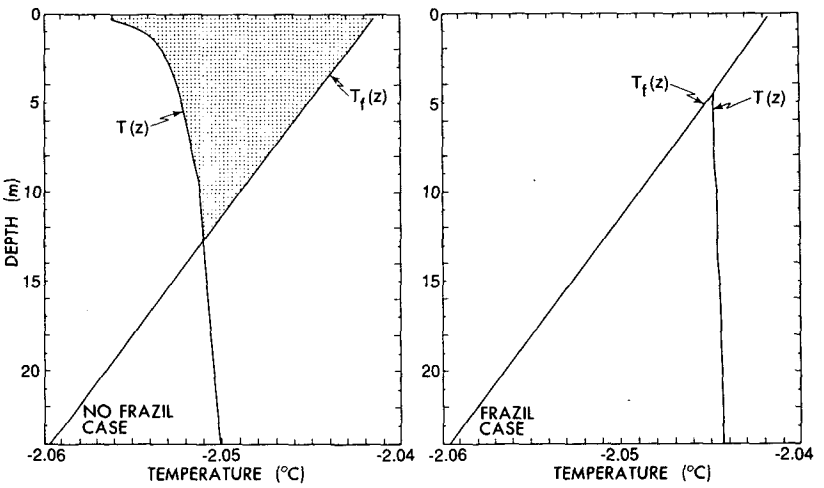

FIG. 5. The vertical thermal structure at four inertial periods, one day after freezing begins. In the left panel, supercooling is allowed to develop (i.e., there is no frazil ice), while in the right panel, frazil ice production is calculated via Eqs. (13)–(15). The shading indicates the region of supercooling, which is limited by the depth-dependence of $T_f(z)$. In the right panel, $T(z) = T_f(z)$ where frazil ice is produced.

We may now solve for any of the three unknowns, γ, T_2 or S_2. The result for γ is

$$\gamma = \frac{-T_{\text{super}}}{\hat{L} + T_1(1 - R) - mS_1} \tag{16}$$

where $T_{\text{super}} \equiv T_1 - mS_1 - nz$. Note that the first term in the denominator, $\hat{L}$, is dominant. To numerically convert this into total precipitated frazil ice thickness, we first note that

$$h_{ik} = \gamma_k \frac{\Delta z_k}{\rho_i / \rho_w} \tag{17}$$

where h_{ik} is the frazil ice thickness at model level k, within a depth Δz_k. The total precipitated frazil ice thickness is thus

$$h_{\text{tot}} = \sum_k h_{ik}. \tag{18}$$

At each time step during the numerical integration, the values T_1 and S_1 generated by the model are replaced by T_2 and S_2, and the total amount of frazil ice is computed.

The change in vertical thermal structure is shown in Fig. 5. The case where frazil ice is produced, and $T(z) = T_f(z)$, is compared with the corresponding case where supercooling is not converted to frazil ice. Figure 6 shows the total ice production, which consists of frazil ice and surface-cooled, or congelation ice. In this experiment, frazil ice makes up about a third of the total. Note that the congelation ice total is essentially unchanged from the experiment of MMS, when frazil ice production was neglected. In Table 1, we list the total ice accumulation at five inertial periods. It will be seen that the Sheppard formulations and the case $b = 0$ are essentially the same and yield little or no frazil ice. For $b > 1.5$ frazil ice production is about a third of the total.

The total amount of ice produced using the four different sublayer parameterizations is not quite the

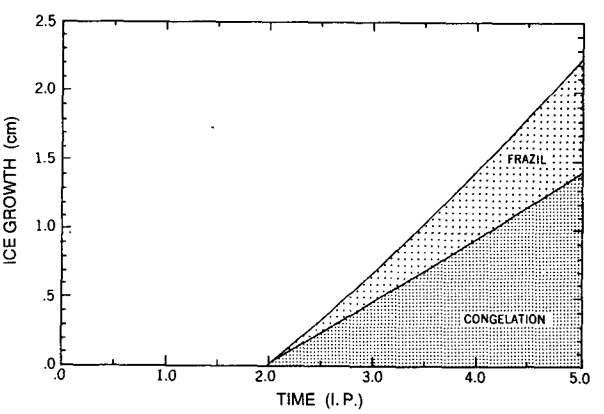

FIG. 6. Total ice production, using the YK sublayer. Congelation, or surface-cooled ice constitutes 1.4 cm of the total by 1.5 days after freezing begins. Frazil ice, formed due to the supercooling of water below the ice, constitutes 0.8 cm of the total by 1.5 days. Freezing is forced by a fixed surface heat sink of 60 W m^{-2}. When the supercooling effect is not converted into equivalent frazil ice production, congelation ice production is nearly identical to that in this figure. When the Sheppard sublayer is used, the congelation ice total at five inertial periods is 2.4 cm, while the frazil ice total is only ~0.03 cm.

same. The vertically integrated thermal balance in the water column is given by

$$\frac{\partial}{\partial t}\int_{-H}^{0} T_f dz = w_c \hat{L}_c + w_F \hat{L}_F - Q_i \qquad (19)$$

where the subscript c denotes congelation and the subscript F denotes frazil ice. The freeze rate is w, and Q_i is the conductive temperature flux through the ice cover. In MMS, $\hat{L}_c$ was defined as $(L/c_{pw})(1 - S_i/S_0)$, where S_i is the salinity of congelation ice, and S_0 is the water salinity at the ice-water interface. Different amounts of heat are released when congelation and frazil ice form, since $\hat{L}_c$ and $\hat{L}_f$ are in general not equal. This effect may be eliminated by setting $S_i = 0$, in which case the totals are identical.

The imposed atmospheric heat sink of $\rho_o c_{po} Q_i = 60$ W m^{-2} assumes a linear temperature profile through 1 m thick ice, varying from −30°C at the surface to approximately −2°C in the water. After several days of additional freezing, Fig. 6 shows new growth of several centimeters. This will tend to decrease the conductive heat flux through the ice, and so reduce the growth rate. The effect is small for initially thick ice. Thinner ice will be more influenced by this negative feedback, so that growth rates will decrease in time. Our experiments also show that the fraction of frazil ice to total ice decreases with decreasing conductive heat flux, so that thin ice (i.e., 10–20 cm) can be composed of ~50% frazil, while thicker ice (80–100 cm) has ~30% frazil. However, further work on this subject demands a more explicit sea-ice model, which is beyond the scope of the present work.

c. *Depth dependence of T_f*

In this section, the effect on ice production of the depth dependence of T_f is investigated. When this term is ignored in Eq. (7), T_f becomes a function of salinity only, which is nearly constant with depth. In this case, frazil ice production is overestimated, since supercooling occurs throughout the water column. By five inertial periods, total frazil ice thickness is 1.1 cm, while in the standard experiment, it is 0.8 cm.

In the ocean, supercooling proceeds for some finite time before frazil nucleation occurs. Figure 7 shows the result of an experiment in which frazil ice production is not permitted until three inertial periods after freezing (and thus supercooling) begins. After an adjustment of ~0.5 day, the estimate of frazil ice thickness is nearly identical to the standard case, wherein frazil ice was created beginning at two inertial periods.

TABLE 1. Ice production at five inertial periods, (in centimeters), for four different parameterizations of the molecular sublayer. When $b = 0$, there is no dependence on molecular Prandtl or Schmidt numbers, and thus supercooling or frazil ice.

		Eq. (6)		
	Eq. (4)	$b = 0$	$b = 1.5$	$b = 3.0$
Congelate ice	2.480	2.510	1.440	1.390
Frazil ice	0.002	—	0.709	0.804
Total	2.482	2.510	2.149	2.194

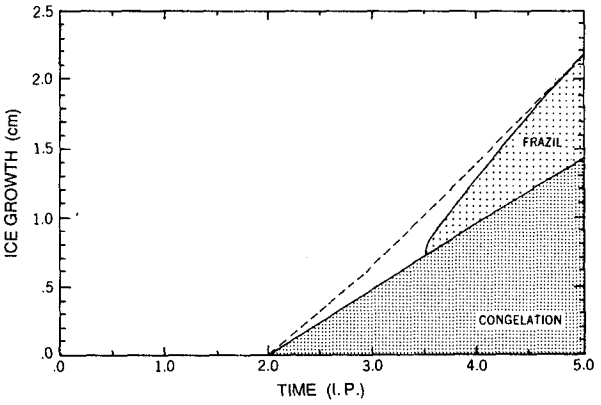

FIG. 7. Total ice production, where frazil ice production is delayed until 3.5 inertial periods. After ~0.5 day, the frazil ice total is nearly identical to that created in the standard case (dotted line), where frazil production began at two inertial periods.

5. Conclusions

The use of a more realistic molecular sublayer parameterization changes the results of the melting and freezing experiments quantitatively, but not qualitatively. In melting, the presence of the YK sublayer slows the melt rate, though the drag coefficient reduction and associated effects are still evident. Also, it allows a mixed layer temperature of ~1.0°C above freezing to coexist with ice melting at less than 5 cm day^{-1}. The freezing case, using the YK sublayer, produces significant supercooling and thus frazil ice formation, in contrast to the tiny amounts predicted in MMS, which used the Sheppard sublayer. The new scheme predicts frazil ice production to be about a third of the total, i.e., frazil plus congelation. Total frazil ice production in this model may be an overestimate, however, considering the simple precipitation scheme employed, as well as uncertainties in the YK formulation itself. On the other hand, an experiment in which ice heat conduction is increased by an order of magnitude, to 600 W m^{-2} yields a larger frazil ice fraction of ~50%.

Observations of the frazil ice fraction in sea ice cores is, in fact, possible, given the different crystal orientations of frazil and congelation ice (Weeks and Ackley 1982). The value varies tremendously from core to core; Weeks and Ackley present fractions from Antarctic cores which range from 5% to 90%! Nonetheless, it seems that the frazil ice component of total sea ice in Antarctica is higher than in the Arctic, and this is sometimes ascribed to the colder Antarctic temperatures at depth. In the present context, this simply means that supercooling occurs faster when $T(z, t = 0)$ is closer to $T_f(z)$. It is unclear at this time, however, how

an actual ice core produced by the concurrent frazil and congelation processes described in this paper would appear.

It is emphasized that the frazil ice mechanism herein described may lead to significant accumulations over several days, even for a relatively low heat sink of 60 W m^{-2}. Another possible mechanism of frazil ice production is direct supercooling of (initially) ice-free leads, where turbulence is maintained by wind mixing. Additionally, supercooling may be produced when water in contact with ice at depth (e.g., pressure keels or ice shelves) rises, due to the depth dependence of T_f discussed above. However, this latter mechanism may be weak away from coasts and especially in the MIZ, where keels are small. And, of course, direct supercooling of leads shuts off as soon as ice begins to accumulate. Thus the significance of the present mechanism, which produces a substantial frazil ice fraction when there exists an ice cover.

Acknowledgments. This work was supported by the Office of Naval Research, Arctic Programs, under Contracts N00014-84-K-0640 (M.S. and G.L.M.) and N00014-84-C-0028 (M.G.M.).

REFERENCES

Fujino, K., E. L. Lewis and R. G. Perkin, 1974: The freezing point of seawater at pressures up to 100 bars. *J. Geophys. Res.*, **79,** 1792–1797.

Garratt, J. R., and B. B. Hicks, 1973: Momentum, heat and water vapour transfer to and from natural and artificial surfaces. *Quart. J. Roy. Meteor. Soc.*, **99,** 680–687.

Josberger, E. G., 1984: Extreme ice edge ablation studies. MIZEX Bulletin, V, 74–75.

Lewis, E. L., and R. A. Lake, 1971: Sea ice and supercooled water, *J. Geophys. Res.*, **76,** 5836–5841.

Lewis, E. L., and R. G. Perkin, 1983: Supercooling and energy exchange near the Arctic Ocean surface. *J. Geophys. Res.*, **88,** 7681–7685.

McPhee, M. G., 1981: An analytic similarity theory for the planetary boundary layer stabilized by surface buoyancy, *Bound.-Layer Meteor.*, **21,** 325–339.

——, G. A. Maykut and J. H. Morison, 1987: Dynamics and thermodynamics of the ice/upper ocean system in the Marginal Ice Zone of the Greenland Sea. *J. Geophys. Res.*, **92,** 7017–7031.

Mellor, G. L., and T. Yamada, 1982: Development of a turbulence closure model for geophysical fluid problems. *Rev. Geophys. Space Phys.*, **20,** 851–875.

——, M. G. McPhee and M. Steele, 1986: Ice-seawater turbulent boundary layer interaction with melting or freezing. *J. Phys. Oceanogr.*, **16,** 1829–1846.

Omstedt, A., and U. Svensson, 1984: Modeling supercooling and ice formation in a tubulent Ekman layer. *J. Geophys. Res.*, **89,** 735–744.

Owen, P. R., and W. R. Thompson, 1963: Heat transfer across rough surfaces. *J. Fluid Mech.*, **15,** 321–334.

Sheppard, P. A., 1958: Transfer across the earth's surface and through the air above. *Quart. J. Roy. Meteor. Soc.*, **84,** 205–224.

Weeks, W. F., and S. F. Ackley, 1982: The growth, structure, and properties of sea ice. *CRREL Monogr.*, **82-1.**

Yaglom, A. M., and B. A. Kader, 1974: Heat and mass transfer between a rough wall and turbulent fluid flow at high Reynolds and Péclet numbers. *J. Fluid Mech.*, **62,** 601–623.